J MATER RES TECHNOL. 2020;9(4):8580–8591

Available online at www.sciencedirect.com

jmr&t Journal of Materials Research and Technology

www.jmrt.com.br

Original Article

Non-grain oriented electrical steel photomicrograph classification using transfer learning

Roberto F. Ivo[a,c], *Douglas de A. Rodrigues*[a,c], *Gabriel M. Bezerra*[b,c], *Francisco N.C. Freitas*[d], *Hamilton Ferreira Gomes de Abreu*[e], *Pedro P. Rebouças Filho*[a,b,c,*]

[a] *Programa de Ps-Graduao em Engenharia de Teleinformtica – Universidade Federal do Cear, Fortaleza-CE, Brazil*
[b] *Programa de Ps-Graduao em Cincia da Computao – Instituto Federal De Educao, Cincia E Tecnologia Do Cear, Fortaleza-CE, Brazil*
[c] *Laboratrio de Processamento de Imagens, Sinais e Computao Aplicada (LAPISCO), Instituto Federal do Cear, Fortaleza-CE, Brazil*
[d] *Programa de Ps-graduao em Energias Renovveis – Instituto Federal De Educao, Cincia E Tecnologia Do Cear, Maracana-CE, Brazil*
[e] *Departamento de Engenharia Metalrgica e de Materiais, Universidade Federal do Cear (UFC), Fortaleza-CE, Brazil*

ARTICLE INFO

Article history:
Received 18 February 2020
Accepted 18 May 2020
Available online 13 June 2020

Keywords:
Non-grain oriented electrical steel
Photomicrograph
Transfer learning
Machine learning

ABSTRACT

Among the many factors that contribute to achieving a sustainable and efficient economy is the raw material of machinery and equipment of strategic sectors. Non-grain oriented (NGO) electrical steel is used in the manufacturing of electric motors. Therefore, it is directly related to the electromagnetic efficiency of engines both in industry and in homes. This work aims to develop an intelligent 1.26% Si NGO electrical steel photomicrograph classification system to assist in the identification of better energy-efficient steel. The concept of Transfer Learning was used to apply Convolutional Neural Network architectures as feature extractors. Traditional machine learning classifiers are applied for coherent categorization of material efficiency. From the results, it is noted that the combination of the InceptionV3 architecture with the k-nearest neighbors classifier reached 100% accuracy and F1-Score. The average extraction time and test time were approximately 15 and 0.920 μs, respectively. Given these results, the literature on this application is surpassed. The best extractor-classifier combination is available in an Internet of Things (IoT) system. Therefore, a professional can freely make use of the proposed approach to assist them in identifying low magnetic loss electrical steel.

* *Corresponding author.*
E-mail: pedrosarf@ifce.edu.br (P.P. Rebouças Filho).
https://doi.org/10.1016/j.jmrt.2020.05.070

1. Introduction

The electrical steel market is forecast to grow at a Compound Annual Growth Rate of around 7.2% for the 2016–2026 period. By the end of this interval, the market is expected to reach US$ 23 billion [1]. Several factors contribute to this optimistic forecast: government and business actions towards a sustainable and efficient economy, the increased popularity of electric and hybrid cars, and the growing need for electricity. Companies are increasingly concerned with the manufacture of quality electrical steel to meet these market demands.

The increase in the number of applications of electrical steels is broad for both types: grain-oriented (GO) electrical steels and non-grain oriented (NGO) electrical steels. Transformers use the first type of steel [2,3], whereas rotors and core stators of electric motors use the second type [4,5].

NGO electrical steels have magnetic properties independent of the direction of the grains. GO electrical steels, on the other hand, have excellent magnetic properties only in the direction of the cold rolling.

The global market has some requirements for the NGO electrical steels: low magnetic loss, high permeability and processability, proper mechanical behavior, and form guarantee. The guarantee of these requirements is related to the procedures performed on the material during manufacturing. NGO electrical steels can be fully processed or semi-processed. The first type is already produced with the ideal characteristics for its final application. In contrast, the second type needs heat treatments performed by the end-user to achieve the desired microstructural features.

After their production, the manufacturing companies have to guarantee the electromagnetic efficiency of these steels. The conventional characterization modes are the study of magnetic hysteresis curves, crystallographic texture maps, or microstructural state [6,7]. Fig. 1 shows these three forms of characterization.

Regarding the microstructure, there is a grain size range for electric steels that present low magnetic losses. According to the work of Shimanaka et al. [8], the ideal grain size is restricted between 100 and 150 μm. Therefore, the electromagnetic efficiency of NGO electric steels is directly related to its grain size. The size is the result of the material's manufacturing process, such as heat treatment and thickness reduction.

However, materials science practitioners have some difficulty in consistently determining the efficiency of the electrical steel of a particular manufacturing process. Several factors contribute to this reality: (1) several parameters are considered during the analysis, so it is not a simple task; (2) it is a repetitive activity; (3) various regions of the material should be analyzed; and (4) the professional's experience is a relevant factor as it requires careful analysis. Thus the analysis is prone to failure due to human error.

Annealing is a heat treatment designed to increase ductility and reduce the hardness of a material. There are three stages in the annealing process: (1) recovery stage, (2) recrystallization stage, and (3) grain growth stage. Burger's work [9] studied the relationship between annealing treatments and electrical steels. The author stated that the most deformed rolled electrical steel showed a smaller grain size in the primary recrystallization.

Several pieces of research in the area of Materials Science have evidenced the application of Computer Science methods to assist professionals and specialists in their tasks, for example, in the characterization of cast iron [10,11] and steel [12–16]. Therefore, companies have turned their attention to this research to develop real-world studies and applications.

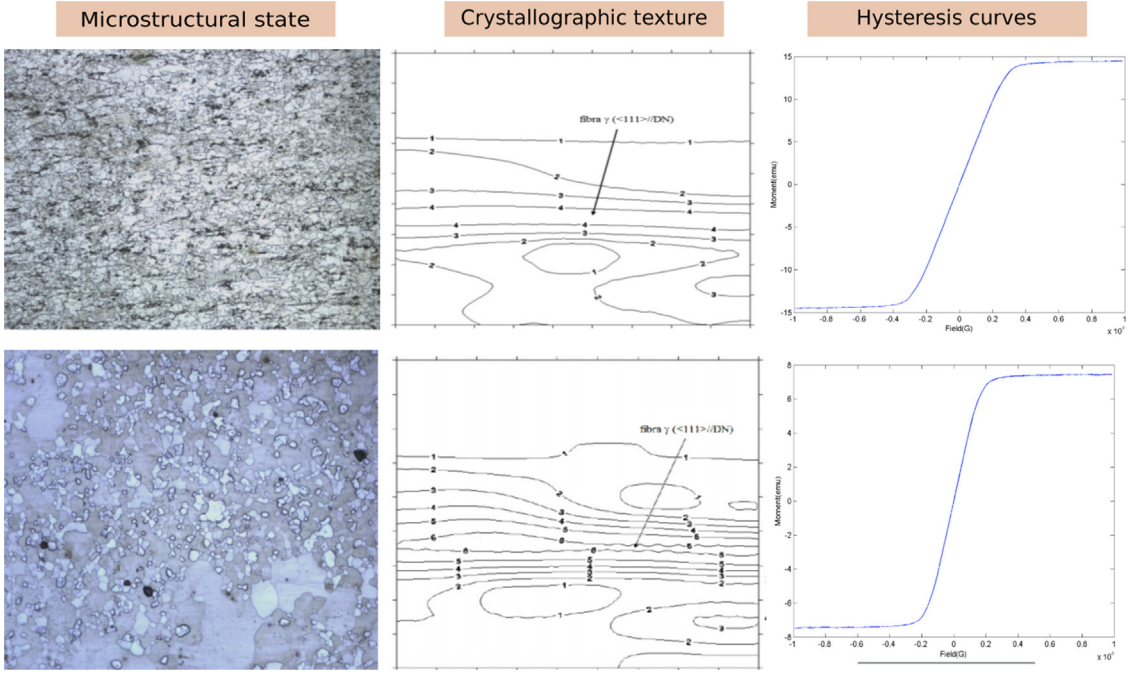

Fig. 1 – Three forms of characterization of NGO electrical steel.

Recent works have investigated approaches to the classification of NGO electrical steel. Filho et al. [12] analyzed the use of traditional image extraction and classification techniques applied to NGO electrical steel photomicrographs, obtaining an accuracy of 97.44%. Ivo et al. [13] use similar techniques, but they are applied to Crystallographic Orientation Distribution Function (CODF) images of NGO electrical steel samples, reaching an accuracy of almost 90%.

Koo et al. [14] proposed the use of Transfer Learning to assess brittle steel fractures automatically. Yang et al. [16] evaluated high-temperature steel alloys by transferring knowledge from an application at room temperature. Also, Mulewicz et al. [15] developed an automatic method of interpretation of steel microstructure, based on the concept of Transfer Learning.

Therefore, the objective of this work is to develop an intelligent, fast and precise method of classifying photomicrographs of NGO electrical steel to assist professionals in the field of materials science in the classification of electric steel as to its magnetic losses, by using an Internet of Things (IoT) system. The proposed approach is motivated by the computational methods that have been successful in techniques in the areas of materials science. As it takes a long time, and several resources are needed to acquire a large number of photomicrographs from NGO electrical steel, we use the concept of Transfer Learning. We apply convolutional neural networks for feature extraction from images and classic machine learning methods for their classification.

The main contributions of this research are shown below:

- It applies the concept of Transfer Learning to a materials science problem, employing adapted CNN architectures as feature extractors.
- It investigates the performance of different machine learning methods as classifiers, using features extracted by CNN architectures.
- It provides a simple online system so that professionals can easily use it as an aid to the classification of electric steel.

2. Methodology

Fig. 2 presents the methodology of this work. Initially, the images of the NGO electrical steel are uploaded to an IoT system (Fig. 2a). Then, the CNN performs the feature extraction (Fig. 2b) and the traditional classifiers perform the classification (Fig. 2c). Finally, the electromagnetic efficiency of electrical steel is predicted (Fig. 2d).

2.1. *Dataset*

The samples used in this work correspond to semi-processed NGO electrical steels with 1.28% silicon (Si). In addition to the percentage of Si in its chemical composition, there is 0.05% carbon, 0.29% manganese, 0.025% phosphorus, 0.014% sulfur, and 0.036% aluminum. The samples were submitted to different treatments, in which the percentage of reduction, the temperature, and the time of treatment varied. The microstructural state of the samples after these different

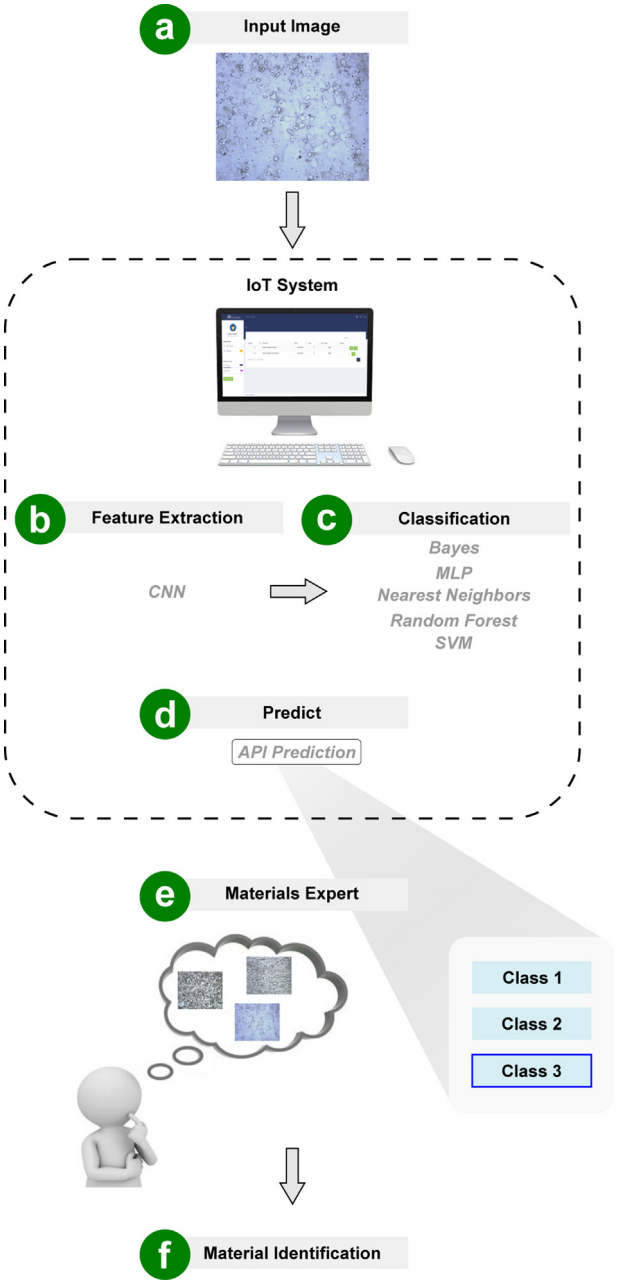

Fig. 2 – Diagram of the proposed approach.

treatments was the criterion used by the specialist to divide the samples into three distinct classes.

The samples belonging to class 1 are those that had 50% reduction and were annealed at 620 °C for 1, 10, 100, and 1000 min and at 730 °C for 1, 10, 100, and 1000 min. Also included in class 1 are samples that have been reduced by 70% and annealed at 620 °C for 1, 10, 100, and 1000 min and annealed at 730 °C for 1, 10, 100, and 1000 min.

The samples belonging to class 2 are those that had a reduction of 50% and annealed at 840 °C for 1, 10, and 100 min, and annealed at 900 °C for 1 and 10 min. Samples with 70% and annealed at 840 °C for 1 and 10 min are also part of class 2.

In class 3, the samples were those that had a 50% reduction annealed at 840 °C for 1000 min and annealed at 900 °C for 100

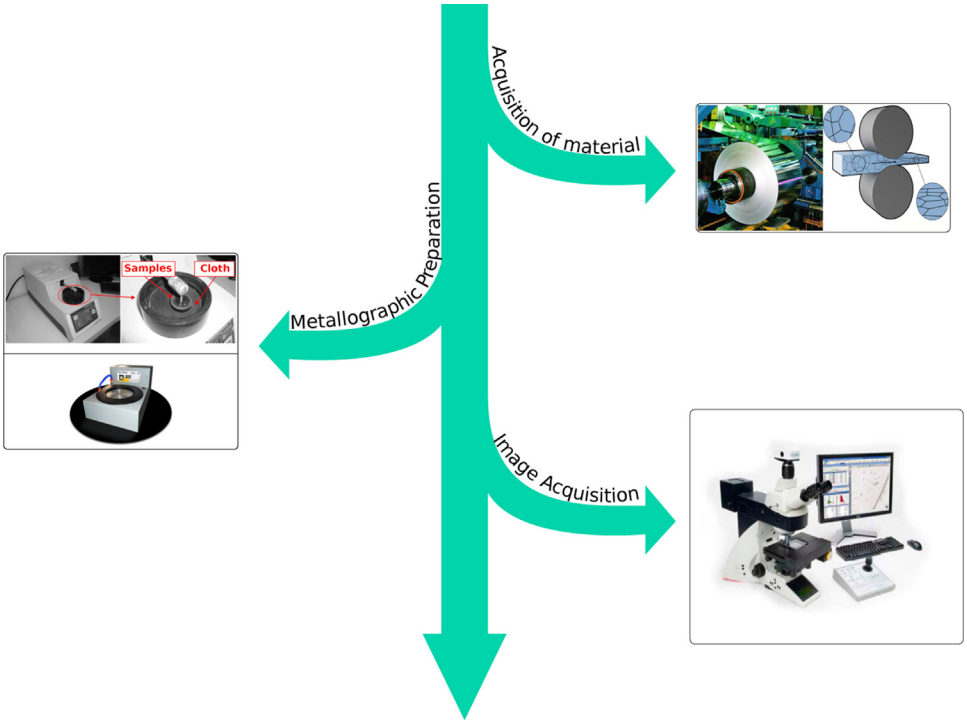

Fig. 3 – Metallographic procedures.

and 1000 min. Also included in the same class are samples that had 70% reduction annealed at 840 °C for 100 and 1000 min, and annealed at 900 °C for 1, 10, 100, and 1000 min.

After heat treatment, sample preparation procedures were performed for microscopic analysis. Fig. 3 shows the entire metallographic preparation process performed. This figure also presents the acquisition of photomicrographs.

Initially, the hot mounting in bakelite was performed, followed by the sanding with different particle sizes sandpaper, subsequently, the polishing with diamond paste. The last procedure was a chemical attack. For image collection, an optical microscope with digital image acquisition was used.

Compared to the initial electrical steel samples, class 1 showed no microstructural modifications, unlike the samples of classes 2 and 3. The second class presented a normal grain growth in its microstructure. In contrast, the microstructure of the third class showed abnormal grain growth, which is typical of secondary recrystallization.

Fig. 4 shows examples of photomicrographs of 1.26% Si NGO electrical steel and their respective classes. In total, the dataset is composed of 127 images.

2.2. *Convolutional neural networks as features extractors*

Convolutional neural networks require a lot of training data [17,18]. We work around this problem by using the Transfer Learning method.

Fig. 5 shows a generic CNN architecture. The operations performed on the input image are divided into layers. The convolution layers perform convolutions of a set of filters with the input matrix, resulting in different feature maps. These feature maps represent the extracted attributes and are the inputs for the next layers [18]. The pooling layers are responsible for reducing the size of the feature maps. Therefore, there is a reduction in the computational cost needed to process the data [19]. After all these layers, the final matrices are transformed into vectors and concatenated. In a standard CNN, this attribute vector is presented to the fully connected layers that are responsible for the classification of the image [20].

To convert CNN models into attribute extractors, we remove the fully connected layers after training the CNN in the extensive ImageNet database. Therefore, each element of the output vector represents a feature extracted from the NGO electric steel image. Thus, a data set was built with the classes of each sample and the extracted attributes, separating this information by the CNN architecture used.

Different configurations of CNN architectures were trained: Visual Geometry Group (VGG), Inception, Neural Architecture Search Network (NASNet), Xception, MobileNet, Residual Networks (ResNet), and Densely Connected Convolutional Network (DenseNet). Table 1 shows the CNN settings used in the project, their main characteristics, and the number of attributes provided by their adaptations.

2.3. *Classifiers*

With the attribute dataset already formed, the classifier training was performed. The classification activity consists of receiving attributes from a sample and then predicting to which class that sample belongs. The classification methods used are described below.

The Bayesian classifier, Nave Bayes (NB), is a supervised method that uses the Bayes Theorem to perform class

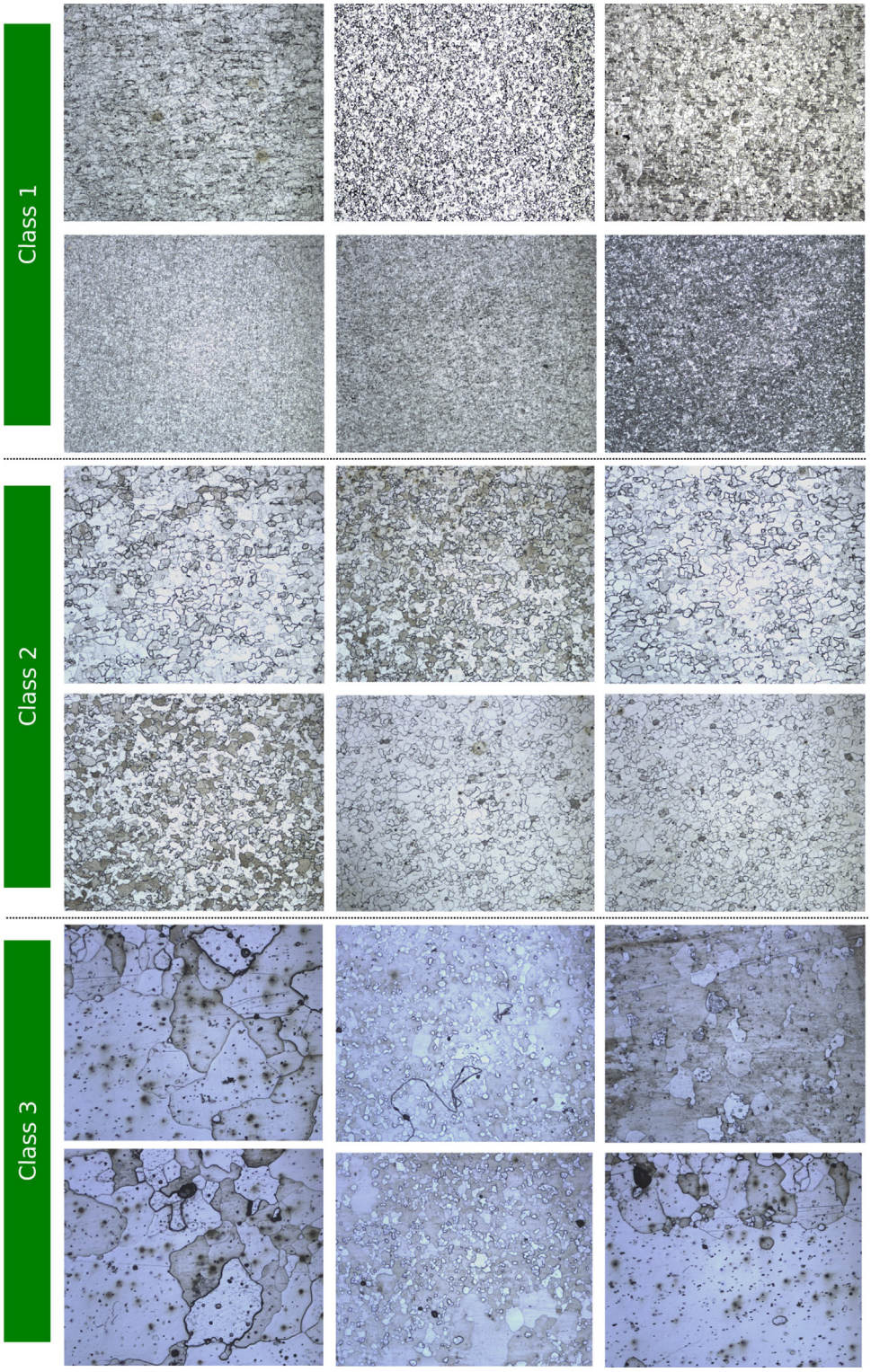

Fig. 4 – Examples of photomicrographs of NGO electrical steel with 1.26% Si and their respective classes.

prediction [28]. To classify a new sample by informing its attributes, it is necessary to calculate the a priori probability of each of the classes and the a posteriori probabilities of each of the attributes given that class. With these values, the a posteriori probabilities of each of the classes are calculated. Thus, the chosen class is the one with the highest probability [28]. The work of Bangaru et al. [29] studied the use of NB to estimate the degree of concrete hydration by microstructural analysis.

Multilayer perceptron (MLP) is a neural network that has an input layer, one or more hidden layers, and an output layer. During the training phase, the outputs are compared to the

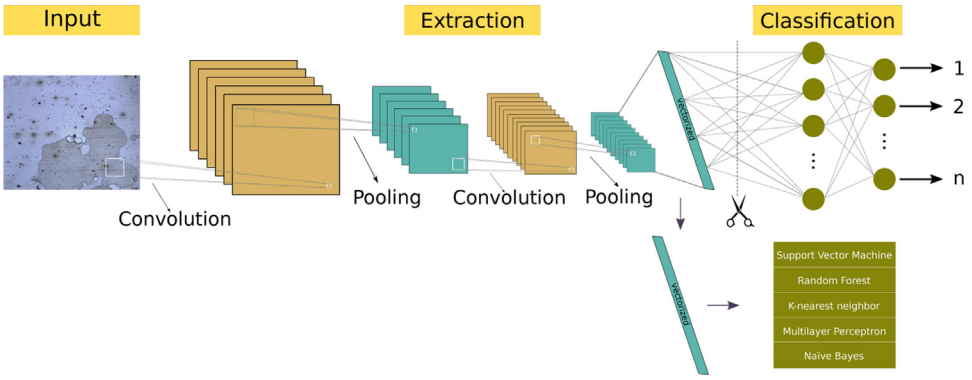

Fig. 5 – Schematic representation of the application of the transfer learning algorithm for the classification of NGO electrical steels.

Table 1 – The characteristics and the number of features returned by each CNN model used in this work.

Architectures	Highlights	Configurations	No. of features
VGG [21]	Factorized Convolution: a regularization strategy to avoid overfitting	VGG16	512
		VGG19	512
Inception [22]	Inception Module: a building block for reducing the amount of extracted parameters	InceptionV3	2048
		InceptionResNetV2	1536
ResNet [23]	Residual Block: a building block focused on optimizing vanishing-gradient	ResNet50	2048
NASNet [24]	NASNet search space: a new architecture model built from the dataset of interest	NASNetLarge	4032
		NASNetMobile	1056
Xception [25]	Depthwise separable convolution: convolution performed independently over each channel, accompanied by a pointwise convolution	Xception	2048
MobileNet [26]	Addition of two news hyperparameters to the Xception model: Width Multiplier and Resolution Multiplier	MobileNet	1024
DenseNet [27]	Dense Block: a block that interconnects all layers	DenseNet121	1024
		DenseNet169	1664
		DenseNet201	1920

desired result, and the net weights are adjusted using the error backpropagation algorithm. Ruelas-Santoyo et al. [30] use MLP to assist in recognition of different carbon steel microstructures through the photomicrograph histogram.

K-nearest neighbor (kNN) is a classification based on the classes of the nearest examples [31]. In kNN, the new sample class will be the most frequent class of the training samples closest to the test sample [32]. The k samples with the shortest distances vote according to their class. Thus, the prediction of the test sample class will be the one that received the most votes. The research by Karthikeyan et al. [33] relies on kNN for the creation of an efficient steel surface defect classification system.

Random Forest (RF) builds several decision trees that are used for classification. These trees are trained using different random subsets of samples and attributes. In the testing phase, each tree votes for one of the classes, and the one with the most votes is the predicted class. Panda et al. [34] propose a carbon steel heat treatment suggestion framework according to the initial and desired microstructure, using the RF classifier.

Support vector machine (SVM) aims to generate a hyperplane as a decision surface, optimizing it to obtain the longest minimum distances between the hyperplane and the examples of different classes [35,36]. SVM has been proposed for low carbon steel microstructure classification [37].

The classifier hyperparameters were determined using a random search with 10-fold cross-validation. For the MLP, the Levenberg–Marquardt method was used, and the number of neurons in the hidden layer ranged from 2 to 1000. In the kNN classifier, odd values from 1 to 9 were used for the number of neighbors k. For the RF training, the criterion was switched between Gini and Entropy, the minimum number of samples required to divide an internal node varied from 2 to 6, the number of trees was fixed at 3000, and the maximum depth was considered to be six or nonexistent. For the SVM classifier, linear, polynomial, and radial basis function (RBF) kernels were used, with the γ and C hyperparameters values of 2^n, with n assuming all integer values between -15 and 3 for γ, or -5 and 15 for C. The only classifier that did not change parameters was the NB, which used a Gaussian probability density function.

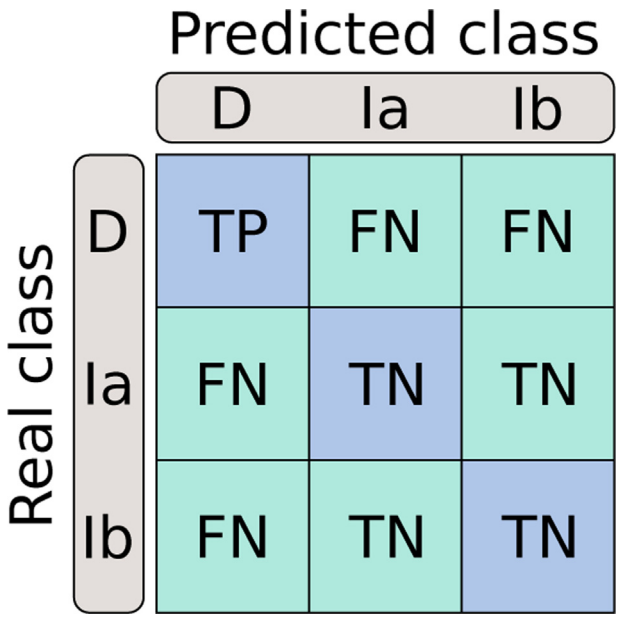

Fig. 6 – The confusion matrix structure.

2.4. *Confusion matrix and evaluation metrics*

NGO electrical steels electromagnetic efficiency classification was evaluated based on the accuracy and F1-Score metrics, and on the extraction time, training time, and test time.

Eqs. (1)–(4) refer to the calculation of the evaluation metrics used in this work. The parameters TN, TP, FN, and FP represent, respectively, the number of true negative, true positive, false negative, and false positive predictions.

$$Acc = \frac{TP + TN}{TP + TN + FP + FN} \tag{1}$$

$$Precision = \frac{TP}{TP + FN} \tag{2}$$

$$Recall = \frac{TP}{TP + FP} \tag{3}$$

$$F1 = \frac{Precision \cdot Recall}{Precision + Recall} \tag{4}$$

A confusion matrix is a tool commonly used in classification problems. This matrix allows the visualization of classifier errors and hits by presenting the actual classes of the samples and the classes predicted for them. In Fig. 6, class D represents the class to be obtained, while Ia and Ib are unwanted classes. Thus, when a sample is predicted as class D, it is considered a *TP* result if the sample is actually from class D, but is considered *FP* if it is from another class. A *TN* result occurs when a sample from class Ia or Ib is predicted as one of these classes. For cases where a sample is predicted as Ia or Ib but belongs to class D, it is considered *FN*.

Accuracy represents the overall performance of the method, indicating how often the classifier is correct. In this case, it indicates how many samples of electrical steel were correctly classified compared to the total amount of samples. Its calculation is presented in Eq. (1).

F1-Score is the harmonic mean of two other metrics: precision and recall. Precision depicts the proportion of correct positive classifications, and Eq. (2) gives its calculation. For example, precision checks how many of the samples classified as the desired electrical steel actually were that type of steel. The recall metric corresponds to the proportion of samples of the desired class that were correctly predicted, and its value is found in Eq. (3). As an example, this metric shows how many samples of the desired electrical steel were classified as an unwanted type. Since the recall metric is as important as precision, the F1-Score metric is evaluated and is given by calculating the harmonic mean of the two, as shown in Eq. (4).

In addition to accuracy and F1-Score, the times of extraction, training, and testing are also analyzed. Extraction time is the time that the adapted CNN takes to return the attribute vector from the moment it receives the image. The training time is counted from the initialization of the classifier until the moment it is assumed that it is ready to perform the classification. On the other hand, the test time is the period it takes for the classifier to receive the attribute vector and predict the class of that image. Therefore, training time is relevant during model building, which is when classifiers are trained. After this step, the extraction and test times become more critical because the sum of the two represents the classification time, which is the duration between receiving the photomicrograph and returning its class.

2.5. *IoT system for NGO electrical steel electromagnetic efficiency classification*

The framework Lapisco Image Interface for Development of Applications (LINDA) was used in all computational steps. This platform allows users to upload a set of images and use the Transfer Learning concept to extract attributes with CNN and then classify images with classic machine learning methods.

This system was created to be an online collaborative network for sharing knowledge of intelligent machines based on deep learning, embedded in the context of IoT [38]. Although the original focus is on the medical field, projects in other areas have been carried out using this platform, such as mobile robot localization [38] and classification of pump vibration patterns [39].

Initially, the user selects on LINDA whether to perform training or prediction. If the first option is chosen, the images must be uploaded to the web service. Then the user selects the desired extractors. In the end, charts and tables present the results for each of the combinations. This way, the user analyzes the performance of the extractors and the classifiers. Then the best combination is chosen and made available as the desired classification system configuration.

If the user initially chooses to perform the prediction only, the required classification system must be informed. Thus, it is only necessary to upload the image, that then the prediction API will return the class to which that sample belongs.

All extraction and training are processed in a computational cloud, with a server located at the Instituto Federal de Educao, Cincia e Tecnologia do Cear (IFCE) in the state of Cear, Brazil.

One of the most significant advantages that this platform has is that it can make the generated classification model

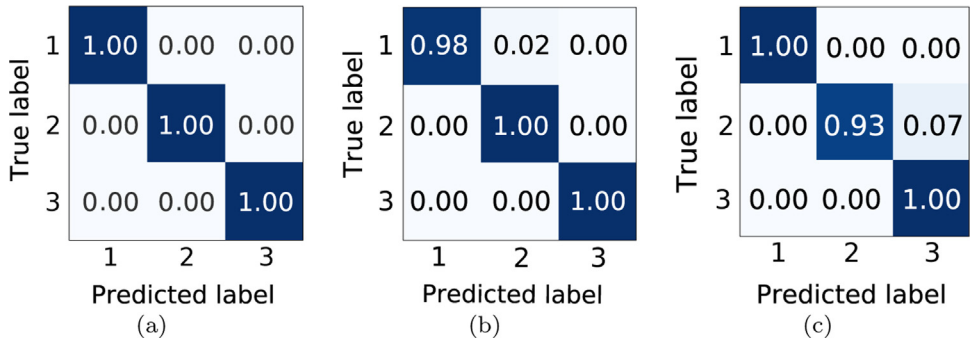

Fig. 7 – Confusion matrices of combinations (a) InceptionV3 with kNN, (b) MobileNet with kNN, and (c) Xception with SVM RBF.

available on the web, allowing others to use it. Also, this model can be easily accessed on different platforms, such as smartphones, allowing professionals to be able to classify NGO electrical steel photomicrographs through their mobile phones.

To access these tools, the user can register for free at [1], informing name, email address, and link to their curriculum. The LINDA interface is intuitive and easy to handle, allowing people with little computer skills, and even no computer vision skills, to classify the images they want.

3. Results and discussion

This section presents and discusses the results obtained by combining the feature extractors with the classifiers applied to the electrical steel images. The extraction, training, and testing steps were performed on a machine with Ubuntu 16.04, Intel Core i5 processor with 3.7 GHz, 16 GB RAM, and GeForce RTX 2060 graphics card with 6 GB RAM.

The average and the standard deviation of accuracy and F1-Score for each of the extractor and classifier combinations are presented in Table 2.

Table 2 shows that all machine learning methods achieved at least 89% accuracy, combined with a specific architecture. The kNN classifier stood out, reaching more than 90% accuracy and F1-Score for all extractors used. Also, it is observed that three combinations achieved average accuracy greater than 98%: InceptionV3 with kNN, MobileNet with kNN, and Xception with SVM RBF. However, the combination that excelled was the InceptionV3 architecture with the kNN classifier, using $k = 1$. This combination pair achieved 100% on both metrics, which means it got all classifications right.

The confusion matrices of these three combinations can be seen in Fig. 7. MobileNet with kNN classified some class 1 samples as class 2, while Xception with SVM RBF classified some class 2 samples as class 3.

The extraction times of each of these three CNN architectures combined with the traditional classifiers are given in Table 3. Also shown in this table are the test and training times for the three best extractor–classifier combinations.

Although the MobileNet and NB combination achieved the shortest test time, 0.080 ± 0.037 μs, its accuracy was only $86.28 \pm 5.54\%$. With the attributes extracted by this architecture, the kNN machine learning method achieved a test time of 0.547 ± 0.020 μs and a training time of 0.711 ± 0.013 μs. Therefore, when presenting a new image, this pair classifies it in less than 3.5 μs. Still, from Table 2, it can be seen that the combination that obtained 100% average classification accuracy, InceptionV3 with kNN, had a test time of only 0.920 ± 0.035 μs. The architecture used in this combination had an extraction time of 14.927 ± 1.449 ms. Thus, a new image presented to this combination is classified in less than 16 ms. The Xception model with the SVM classifier in the RBF configuration achieved 13.680 ± 1.286 μs of extraction time with 56.445 ± 3.171 μs training time and 0.417 ± 0.027 μs test time.

Even though the MobileNet and NB combination obtained the shortest classification time, its accuracy was only $86.28 \pm 5.54\%$. As can be seen from the confusion matrix in Fig. 8, several classifications were incorrect, especially from class 2 samples. Also, the system will generally be applied in an environment in which correct classification is more important than an extremely fast classification. Therefore, the InceptionV3 and kNN combination, which achieved 100.00% accuracy, represents the most appropriate pair for the problem, even though it has an image classification of about 12.5 ms slower than the MobileNet and NB combination.

All of the trained and adapted CNN configurations presented in this paper, and all the classifiers discussed are available on LINDA. Also, the metrics used to analyze performance are made possible by LINDA.

3.1. *Comparison with literature works*

Several works address the use of Digital Image Processing, pattern recognition, transfer learning, and CNN in the field of materials science. However, these researches used these computational methods in materials such as cast iron. As far as we know, through extensive research in the literature, the only works in the literature that perform the classification of NGO electrical steel using the microstructure or the CODF images are, respectively, the works of Filho et al. [12] and Ivo et al. [13].

Filho et al. [12] also used photomicrographs, applying Gray-Level Co-occurrence Matrix (GLCM) as the extractor and kNN

[1] http://lapiscoapi.ifce.edu.br

Table 2 – Accuracy and F1-Score results of the extractor and classifier combinations.

Extractor	Classifier	Accuracy (%)	F1-Score (%)	Extractor	Classifier	Accuracy (%)	F1-Score (%)
MobileNet	NB	86.281 ± 5.541	85.768 ± 5.792	**Xception**	NB	89.223 ± 3.366	88.720 ± 3.748
	MLP	95.095 ± 5.478	94.754 ± 6.087		MLP	95.138 ± 5.220	95.099 ± 5.260
	kNN	**99.048 ± 1.905**	**99.056 ± 1.888**		kNN	96.090 ± 3.596	96.082 ± 3.588
	RF	93.090 ± 5.047	92.737 ± 5.570		RF	95.038 ± 4.496	94.889 ± 4.660
	SVM linear	98.000 ± 4.000	97.943 ± 4.114		SVM linear	96.190 ± 3.563	96.201 ± 3.549
	SVM polynomial	98.000 ± 4.000	97.943 ± 4.114		SVM polynomial	37.995 ± 7.848	24.435 ± 5.016
	SVM RBF	95.143 ± 4.369	95.144 ± 4.371		**SVM RBF**	**98.095 ± 2.333**	**98.082 ± 2.349**
InceptionV3	NB	82.297 ± 5.455	81.738 ± 5.534	VGG19	NB	60.393 ± 4.167	50.311 ± 3.896
	MLP	95.077 ± 4.410	94.819 ± 4.707		MLP	89.238 ± 6.568	88.714 ± 7.082
	kNN	**100.000 ± 0.000**	**100.000 ± 0.000**		kNN	91.138 ± 1.812	91.016 ± 1.843
	RF	91.115 ± 4.807	90.295 ± 5.822		RF	89.233 ± 4.609	88.275 ± 5.430
	SVM linear	93.115 ± 6.682	92.324 ± 7.673		SVM linear	92.143 ± 6.778	91.751 ± 7.385
	SVM polynomial	89.206 ± 5.428	88.365 ± 6.177		SVM polynomial	32.902 ± 7.261	16.708 ± 6.891
	SVM RBF	95.167 ± 6.000	94.703 ± 6.584		SVM RBF	91.190 ± 6.609	90.676 ± 7.192
DenseNet121	NB	85.133 ± 8.845	83.711 ± 9.803	NASNetLarge	NB	87.111 ± 5.814	87.045 ± 5.682
	MLP	93.143 ± 5.065	93.003 ± 5.257		MLP	92.016 ± 2.600	91.859 ± 2.767
	kNN	94.095 ± 3.769	93.860 ± 4.027		kNN	96.143 ± 3.577	96.151 ± 3.575
	RF	89.085 ± 5.778	88.391 ± 6.324		RF	92.968 ± 2.731	92.795 ± 2.899
	SVM linear	97.048 ± 2.412	97.031 ± 2.427		SVM linear	92.810 ± 5.615	92.727 ± 5.704
	SVM polynomial	36.060 ± 13.564	21.386 ± 16.236		SVM polynomial	37.540 ± 7.229	26.291 ± 8.751
	SVM RBF	95.190 ± 5.217	94.896 ± 5.758		SVM RBF	93.810 ± 6.317	93.834 ± 6.235
DenseNet169	NB	84.318 ± 8.048	80.868 ± 11.662	NASNetMobile	NB	75.415 ± 7.962	73.607 ± 8.884
	MLP	95.143 ± 6.101	94.952 ± 6.400		MLP	90.114 ± 7.298	89.845 ± 7.468
	kNN	94.238 ± 6.993	94.121 ± 7.199		kNN	94.933 ± 3.340	94.912 ± 3.399
	RF	92.238 ± 4.869	91.738 ± 5.230		RF	86.305 ± 7.216	85.298 ± 7.961
	SVM linear	94.143 ± 5.613	93.952 ± 5.905		SVM linear	88.200 ± 10.441	88.245 ± 10.281
	SVM polynomial	32.902 ± 7.261	16.708 ± 6.891		SVM polynomial	81.329 ± 7.163	81.205 ± 6.997
	SVM RBF	95.190 ± 5.217	94.992 ± 5.566		SVM RBF	89.157 ± 3.629	88.246 ± 4.547
DenseNet201	NB	87.317 ± 4.674	86.213 ± 5.578	ResNet50	NB	75.333 ± 11.790	74.373 ± 11.857
	MLP	94.190 ± 5.621	94.009 ± 5.902		MLP	89.968 ± 5.592	89.660 ± 5.758
	kNN	94.238 ± 6.993	94.132 ± 7.200		kNN	91.063 ± 3.650	90.954 ± 3.751
	RF	92.333 ± 4.829	92.056 ± 5.130		RF	87.905 ± 5.484	87.513 ± 5.668
	SVM linear	95.143 ± 4.369	95.098 ± 4.409		SVM linear	92.810 ± 4.739	92.849 ± 4.534
	SVM polynomial	28.698 ± 0.720	13.963 ± 2.850		SVM polynomial	43.460 ± 7.475	32.215 ± 6.230
	SVM RBF	93.238 ± 4.916	93.126 ± 5.157		SVM RBF	92.810 ± 4.739	92.849 ± 4.534
InceptionResNetV2	NB	87.024 ± 5.293	85.356 ± 6.595	VGG16	NB	63.467 ± 3.634	53.296 ± 3.893
	MLP	92.933 ± 5.390	92.325 ± 6.234		MLP	93.177 ± 5.005	93.006 ± 5.253
	kNN	92.077 ± 5.090	91.965 ± 5.224		kNN	96.942 ± 4.165	96.748 ± 4.507
	RF	89.933 ± 4.759	88.957 ± 5.676		RF	88.310 ± 5.695	87.434 ± 6.678
	SVM linear	91.986 ± 4.131	91.554 ± 4.797		SVM linear	97.229 ± 3.659	97.223 ± 3.663
	SVM polynomial	55.177 ± 11.006	42.510 ± 12.696		SVM polynomial	31.384 ± 7.381	16.598 ± 7.051
	SVM RBF	90.077 ± 3.196	89.785 ± 3.730		SVM RBF	96.229 ± 3.442	96.223 ± 3.444

Table 3 – Extraction time (ET), training time (TrT), and test time (TsT) for the three combinations of CNN architecture and classifier that stood out in the metrics.

Model	Classifier	ET (μs)	TrT (μs)	TsT (μs)
MobileNet	kNN	3.334 ± 0.276	0.711 ± 0.013	0.547 ± 0.020
InceptionV3	kNN	14.927 ± 1.449	1.185 ± 0.031	0.920 ± 0.035
Xception	SVM – RBF	13.680 ± 1.286	56.445 ± 3.171	0.417 ± 0.027

Table 4 – Comparison of the results obtained between the proposed method and other approaches [12,13].

Work	Acc (%)	F1 (%)	ET (ms)	TsT (ms)
Proposed	**100.00**	**100.00**	**14.92**	**0.00092**
Filho et al. [12]	97.44	98.55	340.00	15.40
Ivo et al. [13]	89.00	80.51	230.00	0.60

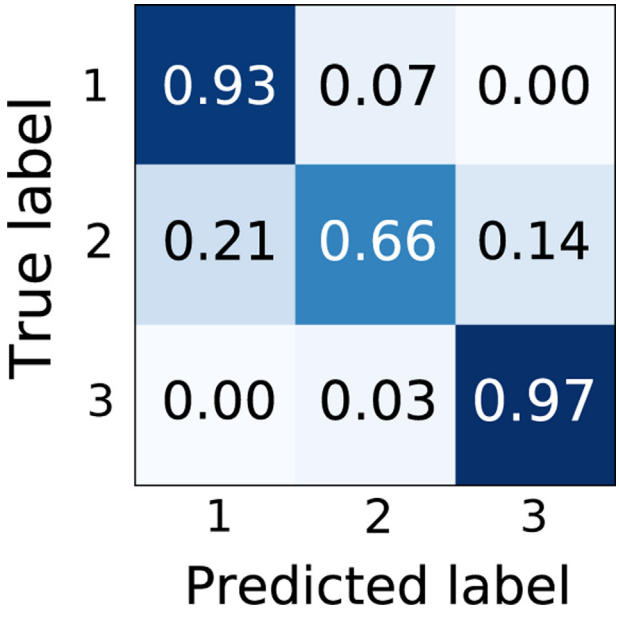

Fig. 8 – Confusion matrix of MobileNet-NB combination.

as the classifier. The authors achieved 97.44% accuracy and 98.55% in the F1-Score. Ivo et al. [13] analyzed another type of image to differentiate the classes: the CODF. The researchers also performed feature extraction with GLCM, but classified images with Polynomial SVM. This approach obtained an average accuracy of 89.00% and an F1-Score of 80.51%.

Table 4 shows the comparison of the results achieved in this work with the results of the only two works that aimed to classify NGO electrical steels. Among the three methods, the one suggested in this paper presents metrics with the best results.

In general, the method proposed in this project presented shorter times than the models suggested in the mentioned works. However, it cannot be said that the proposed system is faster because the extractions, tests, and training were performed using machines with different configurations. Nevertheless, it can be said that it is much more accurate in classification.

4. Conclusion

The paper proposes a new approach to the classification of NGO electrical steel. The method was successful in classifying this type of steel using its photomicrographs. For this, we used CNN architectures based on the concept of Transfer Learning as attribute extractors and machine learning techniques as classifiers. These steps were performed through the LINDA framework, which also enabled the availability of the intelligent classification system for easy online access.

The best performing extractor and classifier combination was the InceptionV3 architecture with the kNN method. This pair showed great results, getting accuracy and F1-Score of 100.00 ± 0.00%. In addition, this combination was also quick, as it had an extraction time of 14.927 ± 1.449 ms, test time of 0.920 ± 0.035 μs, and training time of 1.185 ± 0.031 μs.

The proposed approach obtained higher accuracy than state-of-the-art NGO electrical steel classification methods. Therefore, the project is a useful tool for categorizing this type of steel in terms of its microstructural state. Additionally, the system is available on an online web service and can be used for free. In this way, it can assist researchers and professionals in the field in identifying samples with low magnetic losses, which can then be used in the construction of more energy-efficient electric machines.

In future work, we intend to develop NGO electrical steel classification methods, also using CODF images and hysteresis curves. Also, we want to integrate these two new methods with the one proposed in this paper, aiming at an automatic, fast, and robust system for the classification of NGO electrical steel regarding its level of magnetic losses.

Conflicts of interest

The authors declare no conflicts of interest.

Acknowledgement

This study was financed in part by the Coordenao de Aperfeioamento de Pessoal de Nvel Superior – Brasil (CAPES)

– Finance Code 001. Also Pedro Pedrosa Rebouas Filho acknowledges the sponsorship from the Brazilian National Council for Research and Development (CNPq) via Grants Nos. 431709/2018-1 and 311973/2018-3.

REFERENCES

[1] Acumen Research and Consulting. Electrical steel market – global industry analysis, market size, opportunities and forecast, 2018–2026. https://www.acumenresearchandconsulting.com/electrical-steel-market [Accessed 21 January 2020].
[2] Qiu F, Ren W, Tian GY, Gao B. Characterization of applied tensile stress using domain wall dynamic behavior of grain-oriented electrical steel. J Magn Magn Mater 2017;432:250–9, http://dx.doi.org/10.1016/j.jmmm.2017.01.076.
[3] Chwastek K, Baghel APS, Borowik P, Ram BS, Kulkarni SV. Loss separation in chosen grades of grain-oriented steel. In: 2016 progress in applied electrical engineering (PAEE). 2016. p. 1–6, http://dx.doi.org/10.1109/PAEE.2016.7605105.
[4] Hubert O, Daniel L, Billardon R. Experimental analysis of the magnetoelastic anisotropy of a non-oriented silicon iron alloy. J Magn Magn Mater 2003;254–255:352–4, http://dx.doi.org/10.1016/S0304-8853(02)00850-8. Proceedings of the 15th international conference on soft magnetic materials (SMM15).
[5] da Silva FE, Freitas FNC, Abreu HFG, Gonçalves LL, de Moura EP, Silva MR. Characterization of the evolution of recrystallization by fluctuation and fractal analyses of the magnetic hysteresis loop in a cold rolled non-oriented electric steel. J Mater Sci 2011;46(10):3282–90, http://dx.doi.org/10.1007/s10853-010-5215-8.
[6] Wu W, Cao H, Ou H, Chen Z, Zhang X, Luo Z, et al. Effects of punching process on crystal orientations, magnetic and mechanical properties in non-oriented silicon steel. J Magn Magn Mater 2017;444:211–7, http://dx.doi.org/10.1016/j.jmmm.2017.07.003.
[7] Park June-Soo, Park Jong-Tae. Effect of stress relief annealing temperature and atmosphere on the microstructure and magnetic properties of non-oriented electrical steels. In: 2016 6th international electric drives production conference (EDPC). 2016. p. 288–92, http://dx.doi.org/10.1109/EDPC.2016.7851344.
[8] Shimanaka H, Ito Y, Matsumara K, Fukuda B. Recent development of non-oriented electrical steel sheets. J Magn Magn Mater 1982;26(1):57–64, http://dx.doi.org/10.1016/0304-8853(82)90116-0.
[9] Burgers W. Principles of recrystallization. The art and science of growing crystals; 1963.
[10] de Albuquerque VHC, Cortez PC, de Alexandria AR, Tavares JMR. A new solution for automatic microstructures analysis from images based on a backpropagation artificial neural network. Nondestr Testing Eval 2008;23(4):273–83, http://dx.doi.org/10.1080/10589750802258986.
[11] Rebouças ES, Braga AM, Marques RC, Filho PPR. A new approach to calculate the nodule density of ductile cast iron graphite using a level set. Measurement 2016;89:316–21, http://dx.doi.org/10.1016/j.measurement.2016.04.029.
[12] Filho PPR, dos Santos JC, Freitas FNC, de Araújo Rodrigues D, Ivo RF, Herculano LFG, et al. New approach to evaluate a non-grain oriented electrical steel electromagnetic performance using photomicrographic analysis via digital image processing. J Mater Res Technol 2019;8(1):112–26, http://dx.doi.org/10.1016/j.jmrt.2017.09.007.
[13] Ivo RF, de Araújo Rodrigues D, dos Santos JC, Freitas FNC, Herculano LFG, de Abreu HFG, et al. Study and classification of the crystallographic orientation distribution function of a non-grain oriented electrical steel using computer vision system. J Mater Res Technol 2019;8(1):1070–83, http://dx.doi.org/10.1016/j.jmrt.2018.05.028.
[14] Koo G, Shin C, Choi H, Lee J-H, Kim SW, Yun JP. Automated brittle fracture rate estimator for steel property evaluation using deep learning after drop-weight tear test. IEEE Access 2019;7:145095–103.
[15] Mulewicz B, Korpala G, Kusiak J, Prahl U. Autonomous interpretation of the microstructure of steels and special alloys. In: Materials science forum, vol. 949. Trans Tech Publ; 2019. p. 24–31.
[16] Yang J, Li X, Lu H, Xu J, Li H. An libs quantitative analysis method for alloy steel at high temperature based on transfer learning. J Anal Atomic Spectrom 2018;33(7):1184–95.
[17] Shin H-C, Roth HR, Gao M, Lu L, Xu Z, Nogues I, et al. Deep convolutional neural networks for computer-aided detection: CNN architectures, dataset characteristics and transfer learning. IEEE Trans Med Imaging 2016;35(5):1285–98.
[18] LeCun Y, Bottou L, Bengio Y, Haffner P, et al. Gradient-based learning applied to document recognition. Proc IEEE 1998;86(11):2278–324.
[19] He K, Zhang X, Ren S, Sun J. Spatial pyramid pooling in deep convolutional networks for visual recognition. IEEE Trans Pattern Anal Mach Intell 2015;37(9):1904–16.
[20] Krizhevsky A, Sutskever I, Hinton GE. Imagenet classification with deep convolutional neural networks. In: Advances in neural information processing systems. 2012. p. 1097–105.
[21] Simonyan K, Zisserman A. Very deep convolutional networks for large-scale image recognition; 2014 arXiv:1409.1556.
[22] Szegedy C, Liu W, Jia Y, Sermanet P, Reed S, Anguelov D, et al. Going deeper with convolutions. In: Proceedings of the IEEE conference on computer vision and pattern recognition. 2015. p. 1–9.
[23] He K, Zhang X, Ren S, Sun J. Deep residual learning for image recognition. In: Proceedings of the IEEE conference on computer vision and pattern recognition. 2016. p. 770–8.
[24] Zoph B, Le QV. Neural architecture search with reinforcement learning; 2016 arXiv:1611.01578.
[25] Chollet F. Xception: Deep learning with depthwise separable convolutions. In: Proceedings of the IEEE conference on computer vision and pattern recognition. 2017. p. 1251–8.
[26] Howard AG, Zhu M, Chen B, Kalenichenko D, Wang W, Weyand T, et al. Mobilenets: efficient convolutional neural networks for mobile vision applications; 2017 arXiv:1704.04861.
[27] Huang G, Liu Z, Van Der Maaten L, Weinberger KQ. Densely connected convolutional networks. In: Proceedings of the IEEE conference on computer vision and pattern recognition. 2017. p. 4700–8.
[28] Rish I, et al. An empirical study of the naive bayes classifier. In: IJCAI 2001 workshop on empirical methods in artificial intelligence, vol. 3. 2001. p. 41–6.
[29] Bangaru SS, Wang C, Hassan M, Jeon HW, Ayiluri T. Estimation of the degree of hydration of concrete through automated machine learning based microstructure analysis-a study on effect of image magnification. Adv Eng Informatics 2019;42:100975.
[30] Ruelas-Santoyo EA, Vázquez-López JA, Yañez-Mendiola J, Baeza-Serrato R, Jimenez-García JA, Sanchez-Márquez J. System for the recognition of wear patterns on microstructures of carbon steels using a multilayer perceptron. Ing Invest 2018;38(1):113–20.
[31] Cover T, Hart P. Nearest neighbor pattern classification. IEEE Trans Inform Theory 1967;13(1):21–7.
[32] Duda RO, Hart PE, Stork DG. Pattern classification. New York: John Wiley & Sons; 2012.

[33] Karthikeyan S, Pravin M, Sathyabama B, Mareeswari M. DWT based LCP features for the classification of steel surface defects in SEM images with KNN classifier; 2016.
[34] Panda A, Naskar R, Pal S. An image texture descriptor based machine learning framework for prediction of thermo-mechanic heat treatment process in plain carbon steel. In: 2019 11th international symposium on image and signal processing and analysis (ISPA). IEEE; 2019. p. 169–75.
[35] Haykin S. Redes neurais: princípios e prática. 2nd Edition Porto Alegre: Bookman; 2001.
[36] Vapnik VN. Statistical learning theory. New York: Wiley-Interscience; 1998.
[37] Gola J, Webel J, Britz D, Guitar A, Staudt T, Winter M, et al. Objective microstructure classification by support vector machine (SVM) using a combination of morphological parameters and textural features for low carbon steels. Comput Mater Sci 2019;160:186–96.
[38] Dourado CMJdM Júnior. Reconhecimento de imagens online – uma nova solução baseada em redes sociais colaborativas, Informática aplicada. Fortaleza: Universidade de Fortaleza; 2019.
[39] Hu Q, Ohata EF, Silva FH, Ramalho GL, Han T, Rebouças Filho PP. A new online approach for classification of pumps vibration patterns based on intelligent iot system. Measurement 2019:107138.